Ring Current Effects: Factors Affecting the NMR Chemical Shift of Molecules Adsorbed on Porous Carbons

Alexander C. Forse,[a] John M. Griffin,[a] Volker Presser,[b] Yury Gogotsi,[c] Clare P. Grey[a,d]

[a]Department of Chemistry, University of Cambridge, Lensfield Road, Cambridge CB2 1EW, UK

[b]INM – Leibniz Institute for New Materials & Saarland University, Campus D2 2, 66123 Saarbrücken, Germany

[c]Department of Materials Science and Engineering and A.J. Drexel Nanotechnology Institute, Drexel University, Philadelphia, PA 19104, USA

[d]Department of Chemistry, Stony Brook University, Stony Brook, New York, NY 11794-3400, USA

*Corresponding author. Email: cpg27@cam.ac.uk

Nuclear magnetic resonance (NMR) spectroscopy is increasingly being used to study the adsorption of molecules in porous carbons, a process which underpins applications ranging from electrochemical energy storage to water purification. Here we present density functional theory (DFT) calculations of the nucleus-independent chemical shift (NICS) near various sp^2 hybridized carbon fragments to explore the structural factors that may affect the resonance frequencies observed for adsorbed species. The domain size of the delocalized electron system affects the calculated NICSs, with larger domains giving rise to larger chemical shieldings. In slit-pores, overlap of the ring current effects from the pore walls is shown to increase the chemical shielding. Finally, curvature in the carbon sheets is shown to

have a significant effect on the NICS. The trends observed are consistent with existing NMR results as well as new spectra presented for an electrolyte adsorbed on carbide-derived carbons prepared at different temperatures.

TOC Graphic

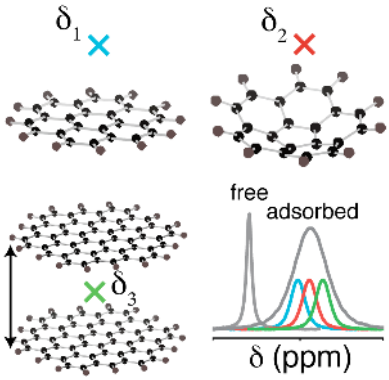

Keywords Nuclear Magnetic Resonance Activated Carbon Supercapacitor DFT Calculations

Introduction

Porous carbons are used in a wide range of applications including the storage of charge in supercapacitors, gas storage, deionization of water, and purification of gases.[1–4] In each case the excellent adsorptive properties of the carbon are exploited to store molecules or ions. Porous carbons are typically prepared by the carbonization and subsequent chemical activation of organic matter such as coconut shells or wood.[5] The resulting amorphous structure consists predominantly of hexagonal carbon rings in which the carbon is sp^2-hybridized.[6] They exhibit a combination of micropores (< 2 nm width), mesopores (2 – 50 nm) and macropores (> 50 nm), and offer extremely high surface areas for molecular adsorption (up to 3000 m^2/g). Porous carbons may also be prepared from inorganic precursors such as metal carbides. In this case, extraction of the metal atoms leaves a porous carbide-derived carbon (CDC) with a pore size that depends on the synthesis conditions.[7–9] Both methods allow the synthesis of carbons with porosity in the nanometer and sub-nanometer range, with CDCs

well known for their narrow pore size distributions that can provide very high adsorption capacities for small gas molecules or electrolyte ions.[10–12]

Nuclear magnetic resonance (NMR) spectroscopy has proven to be a particularly useful technique for studying molecular adsorption inside microporous carbon. When the nuclear spins in the adsorbate are studied, separate resonances are observed for adsorbed and free species.[13–24] Regardless of the nuclear spin studied, resonances arising from adsorbed molecules are shifted to lower frequencies relative to their free counterparts. This is because the species close to carbon surfaces experience a locally reduced magnetic field owing to the circulation of nearby delocalized π electrons in the carbon. As such, to a first approximation such 'ring-current' effects are nucleus-independent.[25] However, if the carbon adsorbent is varied, differences in chemical shielding are observed for a given adsorbate, implying that different carbon structures give rise to different ring-current effects.[15,18]

For a known carbon structure, first-principles calculations can be performed to determine chemical shielding tensors and their isotropic values (σ_{iso}) at arbitrary positions above and around the structure.[26] The isotropic nucleus-independent chemical shift at that position, δ_{iso}^{NICS} (referred to more generally as the NICS here) is then given by $-(\sigma_{iso} - \sigma_{ref})$, where σ_{ref} is zero in this case. While the NICS was introduced as a measure of aromaticity,[27] it may also be interpreted as a measure of the change in chemical shift that may be expected due to the influence of the carbon ring-currents. Such calculations have been performed on idealized carbon systems such as graphene sheets, nanotubes and fullerenes.[28–31] Computed NICS values along a line perpendicular to the molecular plane may be used to obtain the magnitude and size of the ring current loops in the aromatic ring current shielding (ARCS) method via the Biot-Savart law.[32] More generally, the gauge including magnetically induced current (GIMIC) method allows computation of the current density induced by a magnetic field,[33,34] an approach which has been used to understand the aromaticity of fullerenes.[35]

Amorphous carbons exhibit complicated structures thought to consist of curved graphene-like sheets and fullerene-like elements arranged in a highly disordered fashion.[6,36–38] As such, calculations

on the basic carbon building blocks offer a convenient starting point to determine structural properties. For example, Moran *et al*. performed NICS calculations on a series of polybenzenoid hydrocarbons of increasing cluster size, though they did not consider distances from the carbon relevant to molecular adsorption.[39] Inspired by the work of Facelli *et al*.,[40] we recently calculated NICSs on a small graphene-like carbon fragment to interpret the resonance frequencies of electrolyte ions adsorbed in the micropores of an activated carbon supercapacitor electrode.[24] The validity of using finite molecular units to model structural and magnetic properties of bulk graphene has also recently been demonstrated.[41]

In this work, NICS calculations are performed on a series of model carbon fragments to explore the structural factors that affect the resonance frequencies of adsorbed species. First, the effect of the size of graphene-like domains is considered, and is shown to have significant effects on the local magnetic field. We then show that the width of model carbon slit-pores has a considerable effect on the chemical shielding inside the pores due to overlap of the shielding effects from each pore wall. Experimental NMR data is then presented for an electrolyte adsorbed on a series of carbide-derived carbons prepared at different temperatures. Carbons prepared at higher temperatures are shown to bring about a greater chemical shielding for adsorbed ions. This is rationalized by considering the sizes of the graphene-like domains in the carbons and the predictions made by the NMR calculations.

Experimental and Theoretical Methods

1. Density functional theory calculations

All geometry optimizations and NMR calculations were performed using Gaussian 03 software.[42] Geometries were optimized using the B3LYP exchange correlation functional with the 6-31G(d) basis set, following the approach of Moran *et al*.[39] Previous work showed that NICSs calculated near aromatic hydrocarbons do not vary significantly when different basis sets are used.[40] For the case of

slit pores, the optimised structure of circumcoronene ($C_{54}H_{18}$) was used to for each pore wall, separated by a distance, *d*. NMR calculations were performed at the same level of theory and with the same basis set to evaluate the chemical shielding tensors for each atom, as well as for several 'ghost' atoms introduced around the structure. These ghost atoms have no electrons or nuclear charge and simply serve to act as probes of the local effective magnetic field at their position. The calculations generate the isotropic chemical shielding, σ_{iso}. The isotropic nucleus-independent chemical shift, δ_{iso}^{NICS}, is given by $-(\sigma_{iso} - \sigma_{ref})$, where σ_{ref} is a reference shielding which has a value of 0 ppm in this case. Throughout the main text δ_{iso}^{NICS} is referred to as the NICS.

2. Carbon materials

Full details of the syntheses of TiC-CDC and $Ti^{13}C$-CDC powders can be found elsewhere.[21] Briefly, TiC was heated at the desired temperature (600, 800, or 1000 °C) in dry chlorine gas for 3 hours. The sample was then held at 600°C in hydrogen gas for 2 hours to remove chlorine and chloride residues. Samples treated in chlorine gas at a temperature X °C (e.g. 600 °C) are referred to as TiC-CDC-X (e.g. TiC-CDC-600).

For the synthesis of isotopic $Ti^{13}C$-CDC, $Ti^{13}C$ was first prepared by heating a stoichiometric mixture of ^{13}C powder (0.4 g, 99 at%, Sigma Aldrich) and crystalline titanium (1.7 g, ≥ 99.99 at%, Sigma Aldrich; particle size: 5 – 10 μm) at 1550 °C for 12 hours. $Ti^{13}C$-CDC samples were then prepared as described above for TiC-CDC.

Free-standing carbon films were fabricated using the standard method for preparing film electrodes, with a mixture of carbon powder (95 wt%) and polytetrafluoroethylene (PTFE) binder (5 wt%). More details can be found in a publication by Chmiola *et al*.[11]

3. NMR sample preparation

A carbon film piece (6.0 mg) was cut and heated for at least 15 h at 200 °C on a vacuum line before being transferred to an argon glove box. The film piece was cut into small pieces and approximately half of these were packed into a 2.5 mm outer diameter zirconia MAS rotor, before adding ~4 μL of

tetraethylammonium tetrafluoroborate, NEt_4BF_4, (≥ 99.0 %, Sigma Aldrich) 1.5 M in deuterated acetonitrile, D_3CCN, (99.80 %, Eurisotop) electrolyte by micro-syringe. The remaining carbon was then packed before capping the rotor (vespel cap).

4. NMR experiments

All NMR experiments were performed using a Bruker Avance I spectrometer operating at a magnetic field strength of 9.4 T, corresponding to a ^1H Larmor frequency of 400.4 MHz with a Bruker 2.5 mm double resonance probe. Experiments studying electrolyte adsorption were performed at 5 kHz MAS using a spin-echo pulse sequence (90°- τ -180°- τ -acquire) to avoid baseline distortions and to remove background signals associated with the probe. For both ^{19}F and ^1H experiments, spin-echo τ delays of 200 μs were used. For ^{13}C NMR experiments of Ti^{13}C-CDC films a simple pulse acquire experiment was used, and an MAS rate of 15 kHz was used. ^{19}F NMR spectra were referenced relative to neat hexafluorobenzene (C_6F_6) at -164.9 ppm, while ^1H NMR spectra were referenced relative to tetramethylsilane using the CH_3 resonance of liquid ethanol at 1.2 ppm as a secondary reference. ^{13}C NMR spectra were referenced to the tertiary carbon atom in adamantane at 38.5 ppm. For both ^{19}F and ^1H NMR experiments a recycle delay of 3 s was used, found to give quantitative spectra. For ^{13}C NMR experiments a recycle delay of 5 s was used. Radiofrequency strengths of between 100 – 135 kHz were used for all nuclei studied.

Results and Discussion

1. Effect of graphene domain size on the NICS

DFT structure optimizations and NMR calculations were performed in Gaussian 03 software, with the B3LYP exchange correlation functional and the 6-31G(d) basis set. Positions less than 3 Å away from the carbon planes were not considered as it is unlikely that molecules will be able to probe these distances due to the Van der Waals radii of the carbon and the probe molecule. Figure 1a shows NICS values calculated at different heights (*z*) above the ring plane of coronene, with three different positions in the *x*-*y* plane being considered. For all positions studied, negative NICS values were

calculated. The results show that the NMR resonance from a nucleus in a molecule adsorbed above coronene should appear at a lower frequency (to the right hand side of the spectrum) than the resonance from the free molecule. This result is in qualitative agreement with experimental data that consistently reveals shielding effects for species adsorbed in porous carbons.

The magnitude of the calculated NICS is greatest for small distances above the centre of coronene, and at large distances the NICS tends towards zero (Figure 1a). Moreover, as positions more remote from the coronene centre (in the *x*-*y* plane) are considered (see position A to B to C) the magnitudes of the NICSs tend to decrease. For example, the calculated value at 3 Å above the centre of the external 6-membered ring (position C, an 'edge' site) is -3.6 ppm, compared to -4.4 ppm at 3 Å above the central ring (position A).

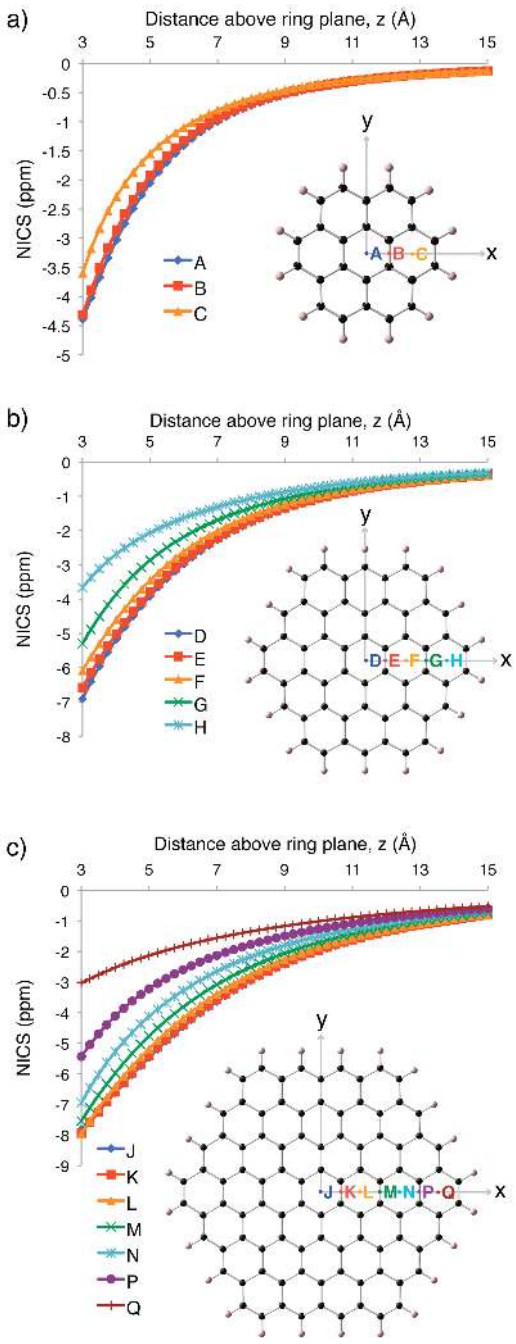

Figure 1: NICS calculations on a) coronene, b) circumcoronene and c) dicircumcoronene. Insets show the optimized structures as well as positions in *x*-*y* where values were calculated.

For carbons derived from both organic and inorganic precursors, the size of the graphene-like domains tends to increase for higher synthesis temperatures.[8,43,44] To explore the effect of the graphene domain size on the NICS, further calculations were performed on a series of coronene-based molecules of larger size. Calculated NICSs for circumcoronene and dicircumcoronene (Figure 1b and

c) show similar trends to coronene, with the largest shielding effects calculated above the ring centres. Importantly, the NICSs above the molecular centres are found to increase with the molecular size. This trend is in agreement with previous NICS calculations used to interpret intermolecular shielding effects in the solid state structures of aromatic molecules.[40,45] Here, the maximum calculated NICS varies from -4.4 to -6.9 to -7.8 ppm as the coronene diameter is increased from 7.5 Å to 12.4 Å to 17.3 Å, respectively. These calculations suggest that a porous carbon with more ordered hexagonal bonding and larger graphene-like domains should bring about greater shielding effects for adsorbate molecules. More disordered carbons with smaller graphene-like domains and more edge sites will result in smaller shielding effects. In real porous carbon particles, a liquid or gaseous adsorbate will experience a range of carbon structures during the NMR timescale at ambient temperatures. Indeed, 2D NMR exchange experiments have shown that electrolyte ions undergo chemical exchange in and out of the carbon micropores on a millisecond timescale.[19,22,23] As such, experimentally observed chemical shifts will arise from a dynamic averaging of chemical shifts associated with many different adsorption sites.

2. Effect of carbon pore size on the NICS

In a porous carbon, molecules may experience the ring-current effects from multiple carbon surfaces within the carbon pores. To probe the effect of well-defined carbon pore sizes on the chemical shifts of adsorbates, NICS calculations were performed on model slit-pores consisting of two individually optimized circumcoronene ($C_{54}H_{18}$) molecules (sheets) separated by a distance, *d* (see Figure 2a). In each case, NICSs were calculated at positions within the pore along the *z*-axis, which coincides with the C_6 symmetry axis, and positions less than 3 Å from the carbon sheets were not considered.

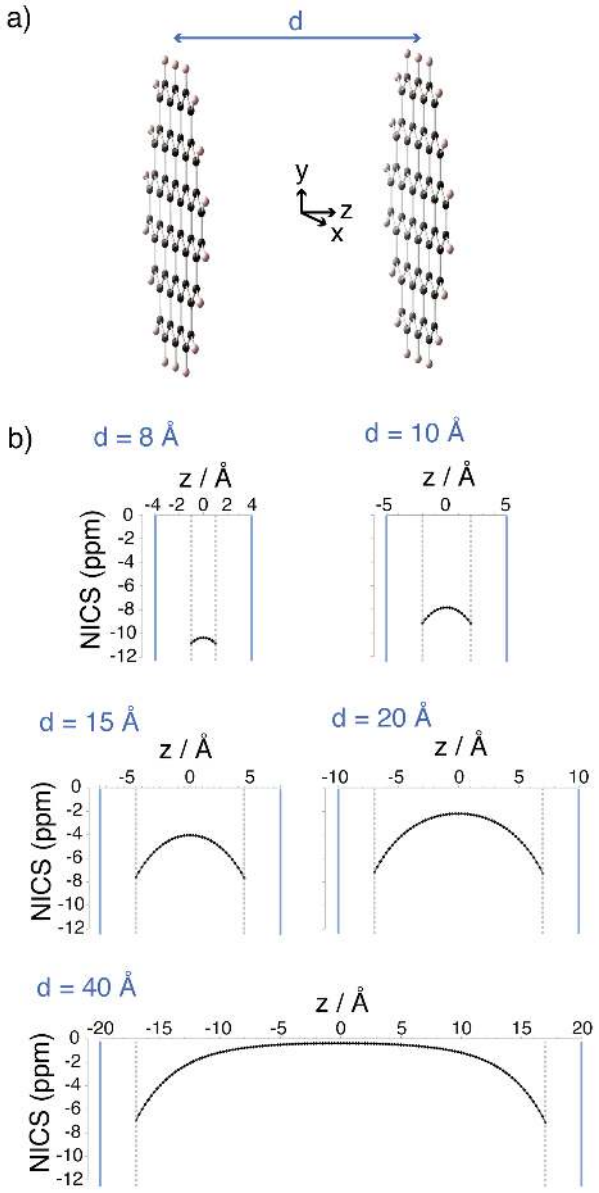

Figure 2: a) geometry of model slit pores comprising two circumcoronene molecules. b) NICS calculations for slit pores with different sizes. Blue solid lines represent the positions of the pore walls. NICS values were calculated between the dotted grey lines.

NICSs are shown in Figure 2b for a range of different pore widths, with negative NICSs calculated for all positions considered. This shows that the NMR resonance from a nucleus in a molecule within a carbon pore should again appear at a lower frequency than the resonance from the free molecule. For small pores (e.g. d = 8 Å), considerable overlap of the shielding effects from the pore walls brings about large NICS values with only small variations across the pore. As the pore size is increased, this

overlap becomes less significant and for a large pore (e.g. d = 40 Å) the overlap is negligible. Importantly, as the pore size is decreased, larger absolute NICS values are calculated. Comparison of the NICS values calculated for the slit-pores with values calculated above a single circumcoronene molecule (Figure 1b) show that the effects of the two circumcoronenes (i.e. the pore walls) are additive to a very good approximation (see Supporting Information). Knowing this, NICS values may readily be generated for a range of different pore sizes given the knowledge of NICS values for a given carbon fragment.

Again, the effects of dynamics must be considered as fast exchange between different adsorption sites will result in an averaging of the observed chemical shift. Indeed, a single NMR resonance was observed experimentally for species adsorbed in a porous carbon with a bimodal pore size distribution, showing that there is fast exchange within the porous network in that carbon.[22] As such it is very reasonable to expect fast exchange between the different positions within a pore. Averaging of the NICSs calculated here yields values of -10.6, -8.3, -5.2, -3.7, and -1.7 ppm for slit (circumcoronene) pores of width 8, 10, 15, 20, and 40 Å, respectively. While it may be more appropriate to perform a weighted average taking into account the effect of the adsorption thermodynamics, the general trend of greater chemical shielding with decreasing pore size will remain unchanged. This qualitative trend agrees well with recent experimental work by Borchardt *et al.*,[22] where magic angle spinning (MAS) ^{11}B NMR spectra of the electrolyte NEt_4BF_4 in acetonitrile (1 M) on a series of carbons with well-controlled pore sizes showed that as the average pore size is decreased the chemical shielding experienced by ions in the pores increases. ^{1}H NMR studies of hydrogen gas adsorbed on a series of activated carbons revealed a similar trend, though in this case carbons with a broader pore size distribution were studied.[18,46] Quantitative comparison of the calculated NICSs with experimental values is difficult, as the ideal slit-pores that we have considered do not capture the more disordered structures of real porous carbons. Moreover, we note that the NICS calculations do not model any changes in the carbon electronic structure due to adsorption.

DFT calculations on molecules confined inside carbon nanotubes have shown that adsorbent-adsorbate interactions can lead to differences between the calculated chemical shifts and the NICSs, though this is generally a minor effect.[29,30] We have observed very similar changes in chemical shift when comparing the ^{11}B, ^{19}F and ^{1}H spectra of BF_4^- and NEt_4^+, suggesting that this effect is small for the carbons/adsorbates that we have studied.[19,21] However, we note that it would be more appropriate to compare shifts from the same adsorbate, when investigating different carbons.

3. Experimental NMR spectra for ions adsorbed on carbide-derived carbons

Previous work has indicated that the ordered domain size of porous CDC increases with synthesis temperature.[38,44] To probe the effect of carbon synthesis temperature on the resonance frequency of adsorbed ions, MAS NMR experiments were performed on a series of titanium carbide-derived carbons (TiC-CDCs) soaked with the electrolyte NEt_4BF_4 in acetonitrile (1.5 M). TiC-CDCs prepared via chlorine gas treatment at 600, 800 and 1000 ºC, denoted TiC-CDC-600, -800 and -1000, respectively, were studied and Figure 3 shows the ^{19}F MAS NMR spectra (see Supporting Information and Ref. 21 for more details on the experimental procedure). For each carbon soaked with electrolyte, two peaks are observed for BF_4^- as in our previous work.[21] Ex-pore resonances arise from anions between primary particles in the carbon film, with a very similar resonance frequency to the neat electrolyte. The in-pore resonances arise from anions adsorbed inside the carbon micropores, shielded by the carbon ring currents. Across the series, the in-pore resonance becomes more shielded, the difference between the in-pore and neat electrolyte chemical shifts varying from -2.6 to -4.0 to -5.4 ppm for TiC-CDC-600, -800 and -1000, respectively. This is despite slight increases in the average pore size (see Supporting Information) of 8.15, 9.06 and 9.32 Å, respectively, which are expected to bring about the opposite effect. The same trend is observed in ^{1}H NMR spectra (this time probing the NEt_4^+ cations) recorded on the same samples (see Supporting Information), showing that the effect is nucleus-independent. We also note that for TiC-CDCs synthesized at higher temperatures, the line

width of the in-pore resonance increases in both the ^{19}F and ^{1}H spectra. This is tentatively ascribed to the increased pore size distributions (see Supporting Information) that would lead to a larger distribution of chemical shifts inside the micropores. Indeed 2D exchange NMR experiments reveal a greater distribution of in-pore environments for TiC-CDC-1000 than TiC-CDC-600 (see Supporting Information).

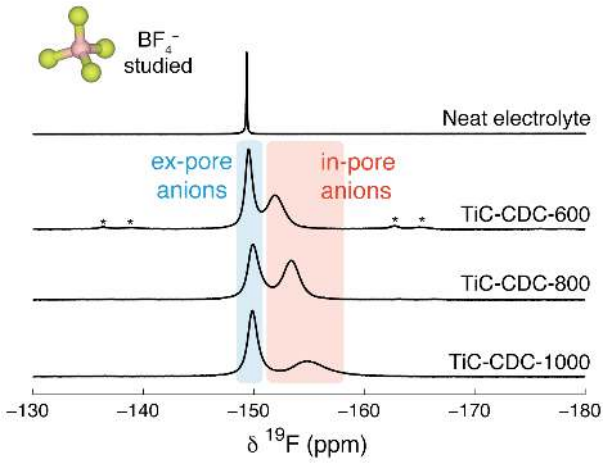

Figure 3: ^{19}F MAS (5 kHz) NMR of different TiC-CDCs soaked with NEt_4BF_4 in acetonitrile electrolyte. Asterisks mark spinning sidebands.

The results agree with recent work where ^{11}B MAS NMR showed that resonances from in-pore BF_4 anions in TiC-CDC-1000 were more shielded than those in TiC-CDC-600.[22] This was rationalized by noting that TiC-CDC-600, with a lower synthesis temperature, is a more disordered carbon with more sp^3-hybridized carbon. In our case, however, we note that ^{13}C NMR experiments on isotopic $Ti^{13}C$-CDC do not show any peaks indicative of sp^3-hybridized carbon, but instead contain only a single broad resonance at ~125 ppm due to sp^2-hybridized carbon (see Supporting Information). Raman spectroscopy (see Supporting Information), magnetic susceptibility measurements,[44] and structural simulations using molecular dynamics[38] show that as the temperature used in the synthesis is increased, the carbon structure becomes more ordered on a local scale with larger graphene-like domains. The calculations presented in Figure 1 then help explain the variation of chemical shift observed for in-pore (adsorbed) ions in carbide-derived carbons, with larger shifts being observed for

carbons with larger graphitic domains. Thus for the case of TiC-CDC, the coherence length of the structural carbon ordering dominates over any pore-size effects.

4. Effect of curvature on the NICS

It has been suggested that non-hexagonal rings in the carbon sheets of porous carbons brings about their curved amorphous structures.[6,36] Indeed, 5-membered rings have recently been detected by transmission electron microscopy of an activated carbon.[47] As such, molecular species adsorbed inside porous carbons may experience a range of different curved carbon structures, as well as planar ones.[48]

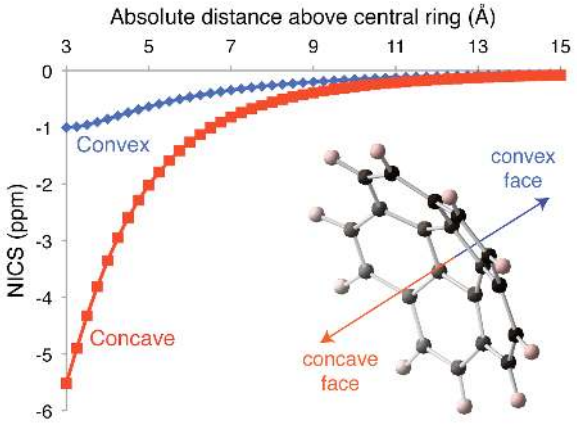

Figure 4: NICS calculations on corannulene.

To probe the effect of curvature on the NICS, calculations were performed on corannulene, which represents a fragment of a fullerene molecule and has a characteristic bowl shape (see inset, Figure 4). NICSs were calculated along the C_5 symmetry axis on both the convex and concave faces of corannulene (Figure 4). On both faces negative NICSs were calculated, though the magnitude of the NICSs are considerably greater on the concave face. While a maximum NICS of -1.0 ppm is calculated on the convex face (at 3 Å from the central ring plane), the maximum NICS on the concave face is -5.5 ppm. The corresponding value for planar coronene is -4.4 ppm (Figure 1a), intermediate between the maximum values calculated for the two faces of corannulene. This suggests that porous carbons exhibiting different amounts of concave, convex and planar surfaces will bring about

different chemical shifts for adsorbed molecules, though the effect of dynamic averaging should again be considered. Deschamps *et al*. recently observed two different NMR environments for adsorbed ions inside activated carbons.[23] In addition to resonances arising from 'type I' ions adsorbed between graphene-like sheets, a less shielded resonance arising from 'type II' adsorption sites was observed and was postulated to arise from ions near 5- or 7-membered carbon rings. Given the results presented here, it is possible that such a type II resonance arises from ions inside regions of the carbon exhibiting a relatively large number of convex carbon surfaces. However, based on the calculations in Figure 1, type II resonances may also arise from ions inside regions of the carbon with more edge sites.

Conclusions

DFT calculations have been used to explore the different structural factors affecting the resonance frequencies observed for species adsorbed in porous carbons. In particular we conclude:

1. Larger graphene-like domains result in greater chemical shielding at distances relevant to molecular adsorption.

2. Smaller carbon slit-pores result in greater chemical shieldings due to overlap of the ring-current effects from each pore wall. These results agree qualitatively with recent experimental data.

3. TiC-CDCs prepared at higher temperatures are shown to bring about a greater chemical shielding for adsorbed ions. This is ascribed to an increase in the structural ordering of the carbon with larger graphene-like domains.

4. Curvature of the carbon surfaces has a marked effect on the NICSs, with convex surfaces bringing about greater chemical shielding than convex surfaces.

We envisage that the observation of these trends will aid the future interpretation of experimental NMR data for molecules adsorbed on porous carbons. Going further, this work offers the possibility of characterizing porous carbons on the basis of the chemical shifts of adsorbed molecules.

Supporting Information

Discussion of additivity of NICSs from pore walls, pore size distributions, ^{13}C NMR and Raman spectra of TiC-CDCs, ^{1}H NMR spectra and ^{19}F 2D exchange NMR spectra of TiC-CDCs soaked with electrolyte. This material is available free of charge via the Internet at http://pubs.acs.org

Notes

The authors declare no competing financial interests.

Acknowledgments

ACF, JMG, and CPG acknowledge the Sims Scholarship (ACF), EPSRC (via the Supergen consortium; JMG) and the EU ERC (via an Advanced Fellowship to CPG) for funding. CDC synthesis at Drexel University was supported by the U.S. Department of Energy, Office of Science, Basic Energy Sciences, under Award #ER46473. VP acknowledges funding from the German Federal Ministry for Research and Education (BMBF) in support of the nanoEES3D project (award number 03EK3013) as part of the strategic funding initiative energy storage framework and thanks Prof. Eduard Arzt (INM) for his continuing support. Mohamed Shamma and Boris Dyatkin (Drexel University) are thanked for their support in the synthesis of CDC material. DFT calculations were performed using the Darwin Supercomputer of the University of Cambridge High Performance Computing Service (http://www.hpc.cam.ac.uk/), provided by Dell Inc. using Strategic Research Infrastructure Funding from the Higher Education Funding Council for England and funding from the Science and Technology Facilities Council. Finally, we thank Hao Wang, Patrice Simon, Phoebe Allan, Nicole Trease, Andy Ilott, Céline Merlet, Beth Howe and Tim Dickens for useful discussions.

References

(1) Simon, P.; Gogotsi, Y. Capacitive Energy Storage in Nanostuctured Carbon-Electrolyte Systems. *Acc. Chem. Res.* **2013**, *46*, 1094–1103.

(2) Porada, S.; Zhao, R.; van der Wal, A.; Presser, V.; Biesheuvel, P. M. Review on the Science and Technology of Water Desalination by Capacitive Deionization. *Prog. Mater. Sci.* **2013**, *58*, 1388–1442.

(3) Ismail, A. F.; David, L. I. B. A Review on the Latest Development of Carbon Membranes for Gas Separation. *J. Membr. Sci.* **2001**, *193*, 1–18.
(4) Candelaria, S. L.; Shao, Y.; Zhou, W.; Li, X.; Xiao, J.; Zhang, J.-G.; Wang, Y.; Liu, J.; Li, J.; Cao, G. Nanostructured Carbon for Energy Storage and Conversion. *Nano Energy* **2012**, *1*, 195–220.
(5) Marsh, H.; Rodriguez-Reinoso, F. Activated Carbon. *1st ed.; Elsevier Science Ltd.* **2006**.
(6) Harris, P. New Perspectives on the Structure of Graphitic Carbons. *Crit. Rev. Solid State Mater. Sci.* **2005**, *30*, 235–253.
(7) Gogotsi, Y.; Nikitin, A.; Ye, H.; Zhou, W.; Fischer, J. E.; Yi, B.; Foley, H. C.; Barsoum, M. W. Nanoporous Carbide-derived Carbon with Tunable Pore Size. *Nat. Mater.* **2003**, *2*, 591–594.
(8) Dash, R.; Chmiola, J.; Yushin, G.; Gogotsi, Y.; Laudisio, G.; Singer, J.; Fischer, J.; Kucheyev, S. Titanium Carbide Derived Nanoporous Carbon for Energy-related Applications. *Carbon* **2006**, *44*, 2489–2497.
(9) Presser, V.; Heon, M.; Gogotsi, Y. Carbide-Derived Carbons - From Porous Networks to Nanotubes and Graphene. *Adv. Funct. Mater.* **2011**, *21*, 810–833.
(10) Sevilla, M.; Mokaya, R. Energy Storage Applications of Activated Carbons: Supercapacitors and Hydrogen Storage. *Energy Environ. Sci.* **2014**, in press, DOI: 10.1039/C3EE43525C.
(11) Chmiola, J.; Yushin, G.; Gogotsi, Y.; Portet, C.; Simon, P.; Taberna, P.-L. Anomalous Increase in Carbon Capacitance at Pore Sizes Less Than 1 Nanometer. *Science* **2006**, *313*, 1760–1763.
(12) Borchardt, L.; Oschatz, M.; Kaskel, S. Tailoring Porosity in Carbon Materials for Supercapacitor Applications. *Mater. Horiz.* **2014**, in press: DOI: 10.1039/c3mh00112a.
(13) Harris, R. K.; Thompson, T. V.; Norman, P. R.; Pottage, C.; Trethewey, A. N. High-resolution 2H Solid-state NMR of 2H2O Adsorbed onto Activated Carbon. *J. Chem. Soc., Faraday Trans.* **1995**, *91*, 1795–1799.
(14) Harris, R. K.; Thompson, T. V.; Norman, P. R.; Pottage, C. Adsorption Competition onto Activated Carbon, Studied by Magic-angle Spinning NMR. *J. Chem. Soc. Faraday. Trans.* **1996**, *92*, 2615–2618.
(15) Harris, R. K.; Thompson, T. V.; Norman, P. R.; Pottage, C. Phosphorus-31 NMR Studies of Adsorption onto Activated Carbon. *Carbon* **1999**, *37*, 1425–1430.
(16) Dickinson, L. M.; Harris, R. K.; Shaw, J. A.; Chinn, M.; Norman, P. R. Oxygen-17 and Deuterium NMR Investigation into the Adsorption of Water on Activated Carbon. *Magn. Reson. Chem.* **2000**, *38*, 918–924.
(17) Lee, S.-I.; Saito, K.; Kanehashi, K.; Hatakeyama, M.; Mitani, S.; Yoon, S.-H.; Korai, Y.; Mochida, I. 11B NMR Study of the Anion in Activated Carbons at Various Stages of Charge of EDLCs in Organic Electrolyte. *Carbon* **2006**, *44*, 2578–2586.
(18) Anderson, R. J.; McNicholas, T. P.; Kleinhammes, A.; Wang, A.; Liu, J.; Wu, Y. NMR Methods for Characterizing the Pore Structures and Hydrogen Storage Properties of Microporous Carbons. *J. Am. Chem. Soc.* **2010**, *132*, 8618–8626.
(19) Wang, H.; Köster, T. K.-J.; Trease, N. M.; Ségalini, J.; Taberna, P.-L.; Simon, P.; Gogotsi, Y.; Grey, C. P. Real-time NMR Studies of Electrochemical Double-layer Capacitors. *J. Am. Chem. Soc.* **2011**, *133*, 19270–19273.
(20) Liu, X.; Pan, X.; Shen, W.; Ren, P.; Han, X.; Bao, X. NMR Study of Preferential Endohedral Adsorption of Methanol in Multiwalled Carbon Nanotubes. *J. Phys. Chem. C* **2012**, *116*, 7803–7809.
(21) Forse, A. C.; Griffin, J. M.; Wang, H.; Trease, N. M.; Presser, V.; Gogotsi, Y.; Simon, P.; Grey, C. P. Nuclear Magnetic Resonance Study of Ion Adsorption on Microporous Carbide-derived Carbon. *Phys. Chem. Chem. Phys.* **2013**, *15*, 7722–7730.

(22) Borchardt, L.; Oschatz, M.; Paasch, S.; Kaskel, S.; Brunner, E. Interaction of Electrolyte Molecules with Carbon Materials of Well-defined Porosity: Characterization by Solid-state NMR Spectroscopy. *Phys. Chem. Chem. Phys.* **2013**, *15*, 15177–15184.
(23) Deschamps, M.; Gilbert, E.; Azais, P.; Raymundo-Piñero, E.; Ammar, M. R.; Simon, P.; Massiot, D.; Béguin, F. Exploring Electrolyte Organization in Supercapacitor Electrodes with Solid-state NMR. *Nat. Mater.* **2013**, *12*, 351–358.
(24) Wang, H.; Forse, A. C.; Griffin, J. M.; Trease, N. M.; Trognko, L.; Taberna, P.-L.; Simon, P.; Grey, C. P. In Situ NMR Spectroscopy of Supercapacitors: Insight into the Charge Storage Mechanism. *J. Am. Chem. Soc.* **2013**, *135*, 18968–18980.
(25) Lazzeretti, P. Ring Currents. *Prog. in Nucl. Magn. Reson. Spectrosc.* **2000**, *36*, 1–88.
(26) Chen, Z.; Wannere, C. S.; Corminboeuf, C.; Puchta, R.; Schleyer, P. v. R. Nucleus-independent Chemical Shifts (NICS) as an Aromaticity Criterion. *Chem. Rev.* **2005**, *105*, 3842–3888.
(27) Schleyer, P. v. R.; Maerker, C.; Dransfeld, A.; Jiao, H.; Hommes, N. J. R. V. E. Nucleus-Independent Chemical Shifts : A Simple and Efficient Aromaticity Probe ReVised Manuscript ReceiVed April 29 , 1996 The Ability to Sustain a Diatropic Ring Current Is the Defining Among Energetic , Geometrical , and Magnetic Criteria of Aroma- Memb. *J. Am. Chem. Soc.* **1996**, *7863*, 6317–6318.
(28) Sebastiani, D. Current Densities and Nucleus-Independent Chemical Shift Maps from Reciprocal-Space Density Functional Perturbation Theory Calculations. *Chem. Phys. Chem.* **2006**, *7*, 164–175.
(29) Kibalchenko, M.; Payne, M. C.; Yates, J. R. Magnetic Response of Single-walled Carbon Nanotubes Induced by an External Magnetic Field. *ACS Nano* **2011**, *5*, 537–545.
(30) Ren, P.; Zheng, A.; Pan, X.; Han, X.; Bao, X. DFT Study on the NMR Chemical Shifts of Molecules Confined in Carbon Nanotubes. *J. Phys. Chem. C* **2013**, *117*, 23418–23424.
(31) Bühl, M. The Relation Between Endohedral Chemical Shifts and Local Aromaticities in Fullerenes. *Chem. Eur. J.* **1998**, *4*, 734–739.
(32) Jusélius, J.; Sundholm, D. Ab Initio Determination of the Induced Ring Current in Aromatic Molecules. *Phys. Chem. Chem. Phys.* **1999**, *1*, 3429–3435.
(33) Jusélius, J.; Sundholm, D.; Gauss, J. Calculation of Current Densities Using Gauge-including Atomic Orbitals. *J. Chem. Phys.* **2004**, *121*, 3952–3963.
(34) Fliegl, H.; Taubert, S.; Lehtonen, O.; Sundholm, D. The Gauge Including Magnetically Induced Current Method. *Phys. Chem. Chem. Phys.* **2011**, *13*, 20500–20518.
(35) Johansson, M. P.; Jusélius, J.; Sundholm, D. Sphere Currents of Buckminsterfullerene. *Angew. Chem. Int. Ed.* **2005**, *44*, 1843–1846.
(36) Harris, P. J. F. Fullerene-like Models for Microporous Carbon. *J. Mater. Sci.* **2013**, *48*, 565–577.
(37) Harris, P. J. F. Structure of Non-graphitising Carbons. *Int. Mater. Rev.* **1997**, *42*, 206–218.
(38) Palmer, J. C.; Llobet, A.; Yeon, S.-H.; Fischer, J. E.; Shi, Y.; Gogotsi, Y.; Gubbins, K. E. Modeling the Structural Evolution of Carbide-derived Carbons Using Quenched Molecular Dynamics. *Carbon* **2010**, *48*, 1116–1123.
(39) Moran, D.; Stahl, F.; Bettinger, H. F.; Scaefer III, H. F.; Schleyer, P. v. R. Towards Graphite : Magnetic Properties of Large Polybenzenoid Hydrocarbons. *J. Am. Chem. Soc.* **2003**, *125*, 6746–6752.
(40) Facelli, J. C. Intermolecular Shielding from Molecular Magnetic Susceptibility. A New View of Intermolecular Ring Current Effects. *Magn. Reson. Chem.* **2006**, *44*, 401–408.
(41) Vähäkangas, J.; Ikäläinen, S.; Lantto, P.; Vaara, J. Nuclear Magnetic Resonance Predictions for Graphenes: Concentric Finite Models and Extrapolation to Large Systems. *Phys. Chem. Chem. Phys.* **2013**, *15*, 4634–4641.

(42) M. J. Frisch, G. W. Trucks, H. B. Schlegel, G. E. S.; M. A. Robb, J. R. Cheeseman, J. A. Montgomery, Jr., T. V.; K. N. Kudin, J. C. Burant, J. M. Millam, S. S. Iyengar, J. T.; V. Barone, B. Mennucci, M. Cossi, G. Scalmani, N. R.; G. A. Petersson, H. Nakatsuji, M. Hada, M. Ehara, K. T.; R. Fukuda, J. Hasegawa, M. Ishida, T. Nakajima, Y. Honda, O. K.; H. Nakai, M. Klene, X. Li, J. E. Knox, H. P. Hratchian, J. B. C.; V. Bakken, C. Adamo, J. Jaramillo, R. Gomperts, R. E. S.; O. Yazyev, A. J. Austin, R. Cammi, C. Pomelli, J. W. O.; P. Y. Ayala, K. Morokuma, G. A. Voth, P. Salvador, J. J. D.; et al. Gaussian 03, Revision E.01.

(43) Zickler, G. A.; Smarsly, B.; Gierlinger, N.; Peterlik, H.; Paris, O. A Reconsideration of the Relationship Between the Crystallite Size La of Carbons Determined by X-ray Diffraction and Raman Spectroscopy. *Carbon* **2006**, *44*, 3239–3246.

(44) Vora, P.; Gopu, P.; Rosario-Canales, M.; Pérez, C.; Gogotsi, Y.; Santiago-Avilés, J.; Kikkawa, J. Correlating Magnetotransport and Diamagnetism of Sp^{2}-bonded Carbon Networks through the Metal-insulator Transition. *Phys. Rev. B* **2011**, *84*, 1–8.

(45) Ma, Z.; Halling, M. D.; Solum, M. S.; Harper, J. K.; Orendt, A. M.; Facelli, J. C.; Pugmire, R. J.; Grant, D. M.; Amick, A. W.; Scott, L. T. Ring Current Effects in Crystals. Evidence from 13C Chemical Shift Tensors for Intermolecular Shielding in 4,7-di-t-butylacenaphthene Versus 4,7-di-t-butylacenaphthylene. *J. Phys. Chem. A* **2007**, *111*, 2020–2027.

(46) McNicholas, T. P.; Wang, A.; Neill, K. O.; Anderson, R. J.; Stadie, N. P.; Kleinhammes, A.; Parilla, P.; Simpson, L.; Ahn, C. C.; Wang, Y.; et al. H2 Storage in Microporous Carbons from PEEK Precursors. *J. Phys. Chem. C* **2010**, *114*, 13902–13908.

(47) Harris, P. J. F.; Liu, Z.; Suenaga, K. Imaging the Atomic Structure of Activated Carbon. *J. Phys.: Condens. Matter* **2008**, *20*, 362201.

(48) Merlet, C.; Péan, C.; Rotenberg, B.; Madden, P. A.; Daffos, B.; Taberna, P.-L.; Simon, P.; Salanne, M. Highly Confined Ions Store Charge More Efficiently in Supercapacitors. *Nat. Comm.* **2013**, *4*, 2701.